Ta–Pt Alloys as Gate Materials for Metal–Oxide–Semiconductor Field Effect Transistor Application

2009 Jpn. J. Appl. Phys. 48 031202

(http://iopscience.iop.org/1347-4065/48/3R/031202)

Ta–Pt Alloys as Gate Materials for Metal–Oxide–Semiconductor Field Effect Transistor Application

Chih-Feng Huang and Bing-Yue Tsui

Department of Electronics Engineering and Institute of Electronics, National Chiao Tung University, ED630, No. 1001, Ta-Hsueh Road, Hsinchu 300, Taiwan, R.O.C.

Received May 18, 2008; revised October 6, 2008; accepted December 14, 2008; published online March 23, 2009

In this work we explore the thermal stability of sputter-deposited Ta-rich Ta–Pt alloys. The effects of group III and V impurities on their work function are also investigated. The Ta content ranges from 65 to 82 at. %. The main phase is σ Ta–Pt. The binding energies of core-level electrons of Ta and Pt are changed due to the intermixing of Ta and Pt, which is evidence that the work function of alloys is changed in metallic alloy systems. Binding energies are thermally stable up to 800 °C. Moreover, the incorporation of Pt in Ta film induces poor crystallization and a compound phase of Ta–Pt alloys. Transmission electron microscopy analysis confirmed the absence of a clear grain boundary in Ta–Pt alloys. The Ta and Pt depth profile shows uniformity in depth after 800 °C annealing for 30 min. The diffusion and distribution of impurities in the alloys were studied by secondary ion mass spectroscopy. Arsenic cannot diffuse in the alloys following annealing at 800 °C for 30 s. In contrast, boron can easily diffuse at 800 °C. The incorporation of impurities with a dosage of 5×10^{15} cm^{-2} in 60 nm Ta–Pt alloy by implantation did not significantly change the flat-band voltage following annealing at 800 °C.

DOI: 10.1143/JJAP.48.031202

1. Introduction

Metal gates have been proposed to replace the polycrystalline silicon (poly-Si) gate beyond the 45 nm technology node in order to solve the problems of gate depletion and boron penetration encountered in the conventional poly-Si gate technology.[1–5] To use a new material to replace poly-Si as the gate electrode, several requirements must be fulfilled. The new gate material must be compatible with the metal–oxide–semiconductor field effect transistor (MOSFET) fabrication process and provide higher device performance. The key requirements for the new material are chemical inertness, immunity to dopant penetration during source/drain ion implantation, and thermal stability during the following high temperature processes.[6,7] Metal gates should have a proper work function (Φ_m) to obtain a suitable threshold voltage for n- or p-type MOSFETs (NMOSFET/PMOSFET),[8,9] where the work function of the metal should be 4.1–4.4 eV for NMOSFETs and 4.8–5.1 eV for PMOSFETs.[8,9] To meet these criteria, refractory metals and their nitrides, such as WN, MoN, TaN, and TiN, have been considered as attractive candidates. However, the work function of most metal nitrides cannot simultaneously satisfy the demands of both NMOSFETs and PMOSFETs. It was proposed that work function modulation over a wide range could be easily carried out using a mixture of two pure metals such as Ta and Pt,[10–12] or Ru and Ta.[13–15] These alloys consist of a metal, Pt or Ru, with a higher work function, and another metal, Ta, with a lower work function. To obtain a high work function, the alloy must contain high atomic concentration of the high-work-function component. On the other hand, an alloy with a high atomic concentration of a low-work-function component exhibits a low work function. The impurities incorporated by the implantation have also been used for effective work function adjustment.[16–18] In particular, the impurities that accumulate at the interface between metal and gate dielectrics can significantly change the effective work function.[16–18] In this work, we examine the thermal stability of Ta–Pt alloys with high Ta concentration. In addition, the electrical effect of incorporating group III or V element impurities on the work function is also studied.

2. Experiments

Simple MOS capacitors with gate electrodes of Ta–Pt alloys were fabricated on 6-in., p-type, (100)-oriented Si wafers. After standard wafer cleaning, a gate oxide was thermally grown to 6 nm in thickness in a dry oxygen atmosphere at 900 °C. After gate oxidation, the alloy gate was patterned by a lift-off process. The 55-nm-thick Ta–Pt alloys were deposited in a co-sputtering system. The sputtering powers of Ta and Pt targets were set to DC 30 and RF 35 W and DC 20 and RF 40 W, respectively. Before lift-off, some samples were implanted with arsenic ions (As^+), phosphorus ions (P^+), or boron difluoride ions (BF_2^+) at a dose of 5×10^{15} cm^{-2}. Then, all samples were capped by a 60-nm-thick silicon nitride film which was deposited at 300 °C by a plasma-enhanced chemical vapor deposition (PECVD) system. The nitride film is used to prevent dopant escape during high-temperature annealing. Samples for electrical analysis were annealed at temperatures from 400 to 800 °C in a rapid thermal annealing (RTA) system for 30 s in a N_2 atmosphere. Typical interlayer dielectric deposition, contact hole patterning, and Al-metallization processes were used to complete the device connect. Finally, a backside contact was formed with an evaporated aluminum film.

For thermal stability analysis, the Ta–Pt alloy sample was deposited on a thin SiO_2 layer in the co-sputtering system with sputtering powers of DC 100 W and DC 30 W for Ta and Pt targets, respectively, to form a Ta-rich alloy film. The annealing temperature ranged from 400 to 800 °C and annealing was performed for 30 min in a horizontal furnace. Table I lists all the samples and process conditions used in this work.

The compositions of the Ta–Pt alloys were determined by Rutherford backscattering spectrometry (RBS). The RBS spectra were obtained using a Van de Graaff accelerator with 2 MeV α particles and calibrated with bulk samples of gold and silicon. The Ta–Pt alloy surface was analyzed using X-ray photoelectron spectroscopy (XPS). The XPS spectra with 0.8 eV experimental resolution were recorded in a Physical Electronics PHI 1600 system, operating at 250 W and 15 keV using a Mg Kα source. A 5 keV Ar^+ ion beam

Table I. Sample ID and process conditions.

	Sample ID				
	A1	A2		A3	
		A2a	A2b	A3a	A3b
Ta target power (W)	DC 100	DC 30	DC 30	DC 20	DC 20
Pt target power (W)	DC 30	RF 35	RF 35	RF 40	RF 40
Implantation	No	No	Yes	No	Yes

was used to etch the sample surface to obtain the bulk XPS spectra. A pure Pt film annealed at 800 °C was analyzed after Ar^+ sputtering to remove surface contamination and the peak of Pt $4f_{7/2}$ at 71.2 eV was used as a binding energy reference obtained from the pure Pt film sputtered from a 99.99% Pt target annealed at 800 °C in a N_2 atmosphere. The alloy phase of the sample was analyzed using X-ray diffraction (XRD). The XRD patterns were obtained with a thin film diffractometer using a Rigaku RU-H3R generator and a scintillation counter. Each sample was irradiated with monochromatic Cu Kα radiation (0.154 nm) generated at 40 keV and 100 mA. The scans were performed over a 2θ range of 30–50° with constant steps of $\Delta(2\theta) = 0.04°$. The pure Pt film deposited from a 99.99% Pt target and annealed at 800 °C in a N2 atmosphere for 30 min was used to correct the peak shift. The microstructure was evaluated by transmission electron microscopy (TEM; Philip Tecnai F20), and the electron diffraction pattern obtained from TEM was used as a supplementary technique to XRD. Auger electron spectroscopy (AES) was used to determine the element depth profile. AES measurements were performed by a VG MicroLab 310F system with an electron-beam energy of 10 keV. Secondary ion mass spectroscopy (SIMS) was used to obtain the impurity depth profile before and after annealing. The SIMS data were collected by a CAMEAC IMS-4F SIMS instrument. During the SIMS analysis, an oxygen ion (O^+) beam was used to sputter the BF_2^+-doped samples and a cesium ion (Cs^+) beam was used to sputter the P^+- and As^+-doped samples. In order to investigate the work function variation caused by the impurity incorporation, the flat-band voltage (V_{fb}) of the MOS structure was extracted from the capacitance–voltage (C–V) curves measured 100 kHz using an Agilent 4284 precision impedance meter.[19)]

3. Results and Discussion

The Ta–Pt phase diagram was reported by Waterstrat in 1981, who identified the main phases to be Ta, ε, σ, PtTa, Pt_2Ta, Pt_3Ta, and Pt.[20)] These phases change from Ta-rich phases to Pt-rich phases with increasing Pt concentration.[21)] The phases of Ta, ε, σ, PtTa, Pt_2Ta, Pt_3Ta, and Pt are present in alloys with Ta atomic concentration of 90.5–100%, 84.5–86.5%, 65–85%, 48.5–50%, 32–33.3%, 24–25.5%, and 0–19%, respectively. In this work, the atomic ratios of Ta/Pt determined by RBS are 74/26, 65/35, and 82/18 for samples A1, A2, and A3, respectively. The work functions previously reported were in the range from 4.7 to 4.5 eV.[10)] The main phase of these alloys is expected to be the σ phase.

3.1 Thermal stability of Ta-rich alloy

Figures 1(a) and 1(b) show the Ta and Pt XPS spectra of the

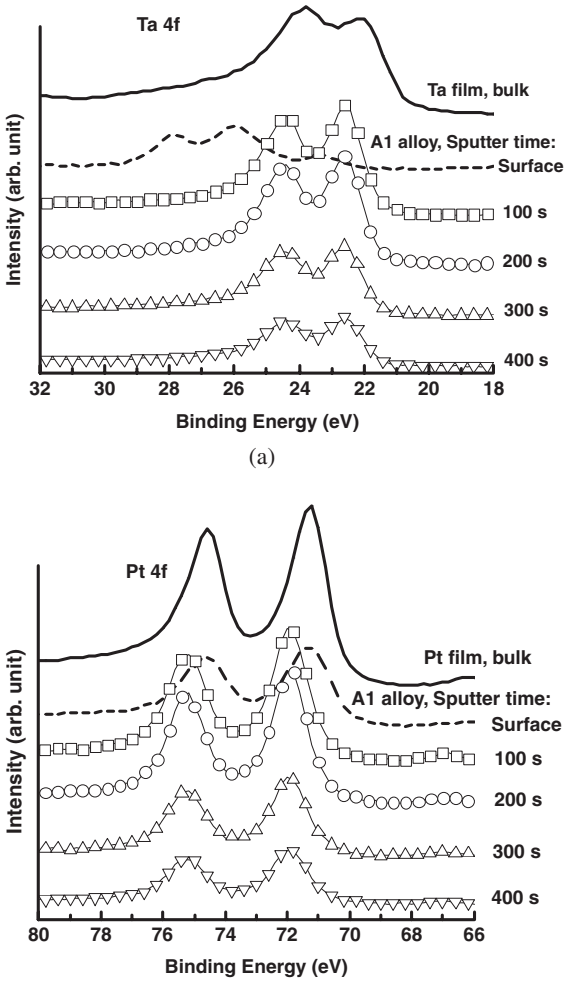

Fig. 1. Binding energies of (a) Ta atoms and (b) Pt atoms of A1 sample after annealing at 800 °C detected by XPS after Ar sputtering for various times. The binding energies of Ta and Pt in pure single metal films are also shown for reference.

A1 sample with Ta–Pt (55 nm)/SiO_2 (6 nm)/Si structure after 800 °C annealing for 30 min. The XPS spectra of pure Ta and Pt films are also shown for comparison. The signals of pure Ta and Pt films have been rescaled by factors of 0.5 and 0.22, respectively. At the sample surface, the binding energy of the $4f_{7/2}$ electron of Ta shifts 3.9 eV from the binding energy of pure Ta $4f_{7/2}$ (22.1 eV) to 26.0 eV. The large shift in the Ta $4f_{7/2}$ electron binding energy is due to the presence of surface oxide (Ta–O bond).[20,23)] The binding energies of Pt are almost identical to those of pure Pt. This is due to the fact that Pt is chemically more inert. The presence of oxidized Ta on the surface is due to exposure to air. After different sputtering periods, the peaks of Ta $4f_{7/2}$ are all located at 22.6 eV (a 0.5 eV shift from pure Ta). The peaks of Pt $4f_{7/2}$ in the TaPt alloys are all located at 71.9 eV indicating a 0.7 eV shift from those of pure Pt. No obvious O 1s signal is observed. The lack of this signal in the bulk of Ta–Pt alloy indicates that the Ta-rich alloys are almost oxygen-free and stable on the SiO_2 film. The work functions of pure Ta and Pt are ~4.3 and ~5.7 eV while TaPt (76% Ta) has a work function of 4.5 eV. The work function change is more than 0.2 eV compared with those of pure elements. The clear shifts of binding energies of Ta and Pt in the Ta–Pt

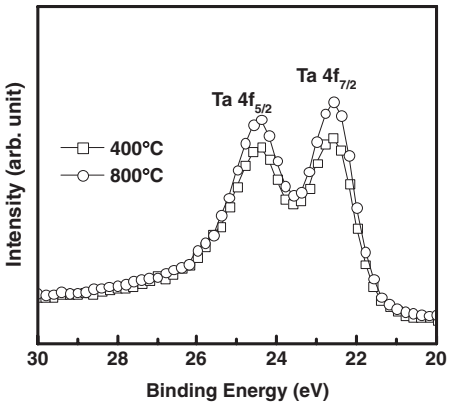

Fig. 2. Binding energies of Ta atoms of the 400 and 800 °C annealed A1 samples detected by XPS after Ar sputtering for 200 s.

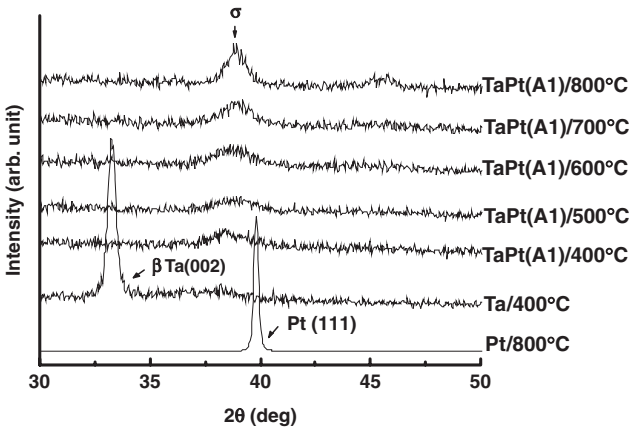

Fig. 3. XRD patterns of the A1 samples after 400, 500, 600, 700, and 800 °C annealing for 30 min. The XRD patterns of pure Ta and Pt films annealed for 30 min are also given for references.

alloy with respect to pure Ta and Pt films imply that Ta and Pt interact with each other to influence the final energy states of the Ta–Pt alloys.[24] It has been postulated that the Ta–Pt alloy forms a new compound with a different work function.[10] This interaction changes the work function of Ta–Pt alloys, depending on the Ta/Pt atomic ratio. The work function modulation due to the element concentration of alloys is greatest for Ru–Ta and Ta–Pt alloy systems which have been applied to complementary MOS (CMOS) applications.[10,13] The binding energies of Ta atoms within the alloy of the 400 and 800 °C annealed A1 samples are shown in Fig. 2, where the signal of the 800 °C sample is that of the 200-s-sputtered sample shown in Fig. 1. The almost identical spectra imply that the alloy is stable up to 800 °C.

Figure 3 shows XRD patterns of pure Pt, pure Ta, and the A1 sample.[25,26] The intensity of the pure Pt film was reduced by a factor of 150. The peak positions of A1 samples after annealing at 400 to 800 °C for 30 min are the same. XRD patterns of pure Ta and Pt metal films were used to distinguish the σ phase from the phases of pure Ta and Pt films. The single peak of the pure Ta film is at 33.24° and the single peak of the pure Pt film is at 39.76°. The peak position of Ta–Pt alloy is different from the peak positions of the pure Ta and Pt films, indicating the formation of the σ Ta–Pt phase. The calculation of d-spaces (the distance between

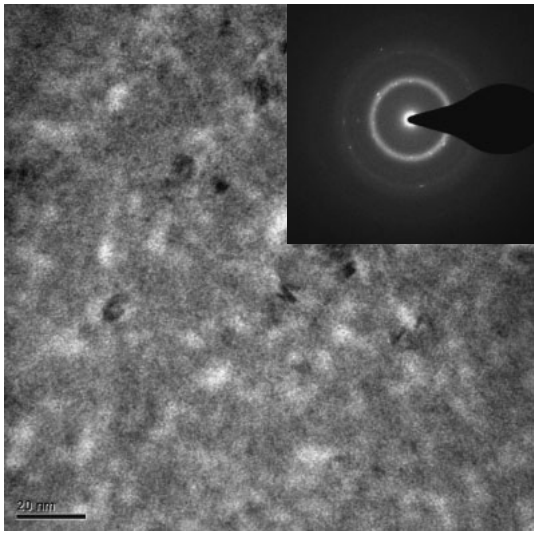

Fig. 4. TEM plane view of the A1 sample annealed at 800 °C for 30 min. The inset shows its relative TEM diffraction pattern.

adjacent planes of atoms) according to Bragg's law showed the d-spacing of peak $2\theta = 38.86°$ was 0.232 nm. The corresponding d-spacing for the peaks of pure Ta and Pt are 0.269 and 0.226 nm, respectively. The diffraction peak of A1 samples is very broad, implying that the grain size of A1 samples is very small. The average grain size can be quantified by the Scherrer equation.[27] The calculated average grain size of A1 samples obtained from the peak at $2\theta = 38.86°$ increases from 4.37 to 8.95 nm as the annealing temperature increases from 400 to 800 °C. The grain sizes of the Ta films annealed at 400 and 800 °C are 21.11 and 39.77 nm, respectively. These results indicate that incorporation of Pt in the Ta film can markedly reduce the grain size.

A TEM diffraction pattern was used to double-check the results of XRD analysis. As shown in Fig. 4, only a broadened diffraction ring was clearly observed for the A1 sample annealed at 800 °C and the corresponded d-space is 0.236 nm, which is similar to the value obtained from XRD analysis. The diffraction points originate from the Si substrate. The broad XRD patterns and the absence of a lattice structure in the TEM diffraction pattern also suggest a poorly ordered crystal. The fact that XRD intensity increases and peak width decreases upon annealing would suggest that annealing induces crystalline ordering. The poorly crystallized Ta–Pt alloy does not form any clear grain boundary, which is always the diffusion path of impurities. Ta–Pt alloys may be a good diffusion barrier. The peak at 45.56° is only observed in the 800 °C XRD spectrum, while it is not observed in the TEM diffraction pattern. The major difference between the XRD sample and the TEM sample is that the surface of the TEM sample was sputtered during preparation. Therefore, the peak at 45.56° in the 800 °C XRD pattern presumably originates from the sample surface. The surface of the XRD sample is oxidized during exposure to air and the XPS analysis indicates the presence of tantalum oxide and pure Pt as shown in Fig. 1. Considering the diffraction patterns of tantalum oxide and Pt, this peak is close to that of Pt(200), which is the second most intense phase in Pt powder.[28] Therefore, the peak at 45.56° in the

Table II. Material characteristics of Ta, Ta–Pt (A1), and Pt films.

Thin film	Phase (orientation)	d-spacing (nm)	Grain size (nm)	Binding energy (eV)	
				Ta $4f_{7/2}$	Pt $4f_{7/2}$
Ta/400 °C	β-Ta(002)	0.269	21.11	22.1	—
Ta–Pt (A1)/400 °C	σ	0.232	4.37	22.6	71.9
Ta–Pt (A1)/800 °C	σ	0.232	8.95	22.6	71.9
Pt/800 °C	Pt(111)	0.226	39.77	—	71.2

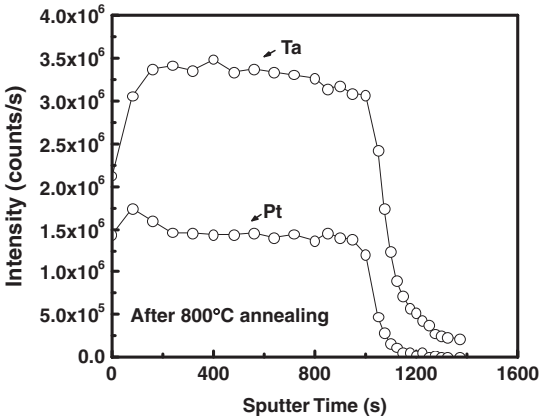

Fig. 5. Depth distribution of the Ta and Pt atoms of the 800 °C annealed A1 samples detected by AES.

800 °C XRD spectrum is presumably due to the presence of Pt(200). The material characteristics of the A1 sample are summarized in Table II.

The composition profile of the Ta–Pt alloy detected by AES is shown in Fig. 5. Since there is no standard for Ta–Pt alloys, the atomic ratio cannot be accurately determined by the AES. Since the average atomic ratios have been determined by RBS, the AES is used to detect the composition uniformity of the alloy film following high-temperature annealing. The AES depth profile shows that the atomic composition of both Ta and Pt of the 800 °C annealed samples is almost constant, except at the sample surface. The AES signals at the surface are disturbed by the surface oxide, as confirmed by the XPS results.

3.2 Effects of impurity incorporation on work function

The C–V characteristics of the 800 °C annealed A3a and A3b samples are shown in Fig. 6. Curves of the implanted samples are slightly smoother than that of the unimplanted sample. The distortion and slightly higher inversion capacitance of the un-implanted curve originate from the high interface states. The effect of III or V impurity incorporation on the work function of alloys is carefully investigated by change in the flat-band voltage (V_{fb}). V_{fb} is defined as

$$V_{fb} = \Phi_{ms} - \frac{Q_{eff}}{C_{ox}}, \quad (1)$$

where Φ_{ms} is the work function difference between the metal gate and silicon substrate, and Q_{eff} and C_{ox} are the effective oxide charges and oxide capacitance, respectively. The deviation of C_{ox} is less than $\pm 5\%$ in this work, and equivalent oxide thickness (EOT) is $\sim$6 nm, which could

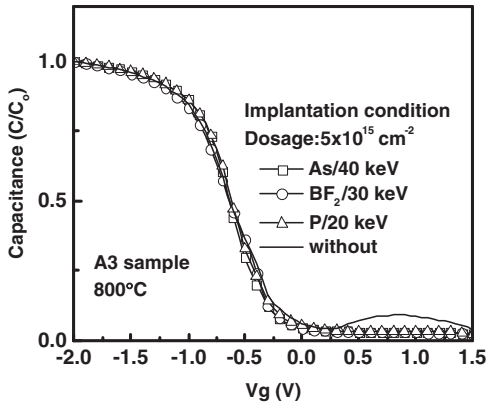

Fig. 6. C–V characteristics of the 800 °C annealed A3 samples with and without ion implantation.

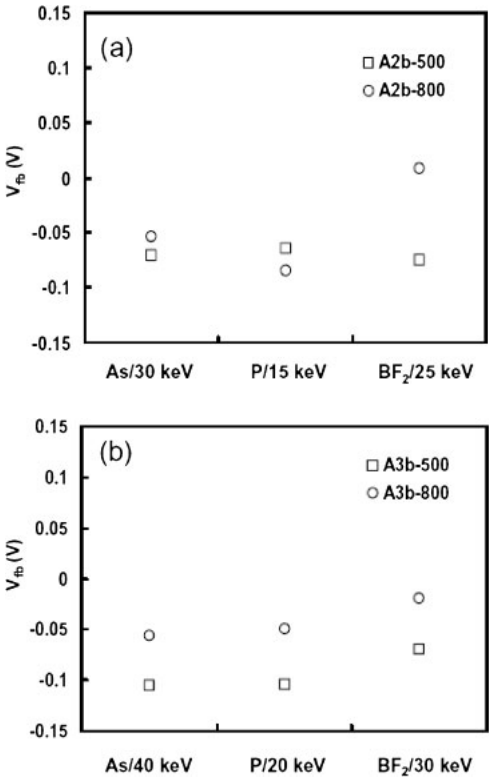

Fig. 7. Flat-band voltage shift (ΔV_{fb}) of (a) A2b samples and (b) A3b samples for various implantation conditions after 500 and 800 °C annealing for 30 s. ΔV_{fb} is the difference between the flat-band voltage of the unimplanted and implanted samples.

have caused only a 100 mV shift in V_{fb} given the very high oxide charge density of $\sim 3.5 \times 10^{11}$ cm^{-2}. Neglecting the deviation of V_{fb} caused by Q_{eff} and C_{ox}, the variation of V_{fb} can reflect the change of work function of metal gate since the silicon substrate is the same for all samples.

The shift of flat-band voltage (ΔV_{fb}) is shown in Fig. 7 for various implantation conditions after annealing at 500 and 800 °C. ΔV_{fb} is defined as the difference in flat-band voltage between implanted samples and unimplanted samples. In Fig. 7(a), ΔV_{fb} for almost all the A2b samples is <0.1 V, i.e., including As^+, BF_2^+, and P^+ implantation. Changing the annealing temperature from 500 to 800 °C affects ΔV_{fb} by less than 0.02 V. Similar results are observed for the

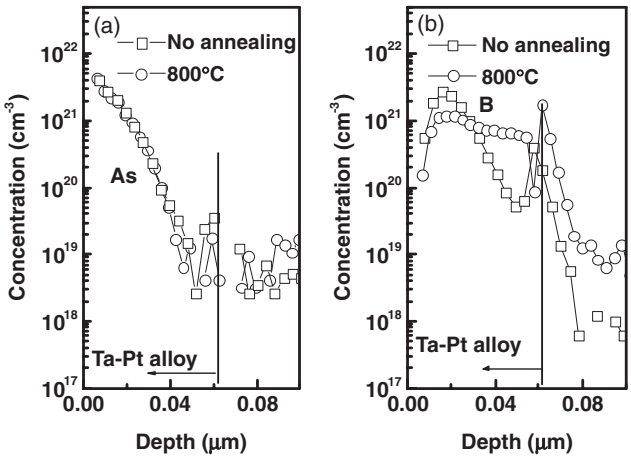

Fig. 8. Depth distributions of the (a) arsenic- and (b) boron-implanted A3b samples before and after 800 °C annealing for 30 s detected by SIMS. The energies of implantation are 50 and 30 keV for As^+ and BF_2^+, respectively, and both dosages are 5×10^{15} cm^{-2}.

A3b sample with higher implantation energy as shown in Fig. 7(b). The ΔV_{fb} of A3b samples are approximately −0.1 V for 500 °C annealed samples and −0.05 V for 800 °C annealed samples.

The impurity distribution can play an important role in determining the effective work function. In particular, the impurity at the interface between the dielectric and the metal gate significantly affects the effective work function due to charge exchange among elements at the interface.[16–18] Although, in this particular case, impurities in Ta–Pt alloys do not significantly change the effective work function or V_{fb}, verifying the impurity profile is still an aid to understanding impurity diffusion and distribution in alloys. The impurity in the alloy was analyzed by secondary ion mass spectroscopy (SIMS). Figure 8(a) shows that the arsenic depth distributions of the A3b samples are almost the same before and after 800 °C annealing. No arsenic is found near the interface between the metal gate and the silicon dioxide, which indicates that the small change of V_{fb} was not related to impurities-induced change in the effective work function. For the BF_2^+-implanted samples, boron impurities are distributed near the surface of the alloy before annealing, and then diffuse and redistribute throughout the alloy film after 800 °C annealing as shown in Fig. 8(b). The depth distributions of P^+-implanted samples before and after annealing are also similar to the case of boron. Although the impurities of boron and phosphorus diffuse in the alloy films, there is no clear evidence of boron and phosphorous accumulated at the Ta–Pt/SiO_2 interface. Only one data point at Ta–Pt/SiO_2 the interface is higher than the SIMS data obtained from bulk, which is thought to originate from the artificial signal at the interface obtained from SIMS analysis. Considering the effect of oxide charges, which was related to the slight distortion of C–V curves in Fig. 6, the effect of the boron dopant on ΔV_{fb} should be much smaller than 100 mV.

The accumulation of impurities at the interface between the metal and SiO_2 may be more efficiently for changing the effective work function, since the effective work function is significantly affected by the interface characteristics. Using the impurities to adjust the effective work function will require high impurity density at the interface. The implanted dose is 5×10^{15} cm^{-2} in 60 nm Ta–Pt film. The concentration of boron impurity may be as high as 5×10^{20} cm^{-3} at the Ta–Pt/SiO_2 interface after annealing at 800 °C. However, such a high impurity concentration cannot significantly change ΔV_{fb}. A higher implantation dosage is needed to increase the change of effective work function or ΔV_{fb}. Boron and phosphorus can easily diffuse in alloys. However, an annealing temperature higher than 850 °C will cause the boron penetration to increase since the gate dielectric is not a good diffusion barrier of boron, as reported for the case of boron doped poly-Si gate.[29] The use of accumulated impurities at the interface to adjust the work function will require a dielectric with the ability to act as a diffusion barrier.

4. Conclusions

The Ta–Pt alloy with an adjustable work function is a suitable material for metal gates because of its stable film structures, and stable work function. The core-level electron binding energy of Ta and Pt was changed by forming a mixture of Ta and Pt reflecting the change of work function. No clear grain boundary was observed by TEM, and a grain size of less than 10 nm following annealing at 800 °C was observed by XRD analysis. The Ta and Pt profile was also observed to be uniform following annealing at 800 °C by Auger analysis. All these characteristics suggest that Ta–Pt alloys are thermally stable up to 800 °C. A dosage of 5×10^{15} cm^{-2} arsenic, boron, or phosphorous was implanted into Ta–Pt alloys while arsenic cannot diffuse in the alloys at 800 °C, boron and phosphorus can easily diffuse. The effect of implanted impurities on V_{fb} is not significant following annealing at 800 °C anneal for 30 s. Although boron and phosphorus can easily diffuse in alloys, no clear boron or phosphorous was accumulation at the interface was observed. Increasing the impurities at the interface between the metal gate and the gate dielectric may help to adjust the effective work function, but a gate dielectric with of the ability to act as a diffusion barrier preventing impurities entering the channel and the gate dielectric will be required.

Acknowledgements

This work was supported by the National Science Council of the R.O.C. under contract NSC 95-2221-E-009-302-MY3. Devices were fabricated at the Nano Facility Center (NFC) of NCTU, Taiwan, R.O.C.

1) International Technology Roadmap for Semiconductors (ITRS) 2003 Edition, Semiconductor Industry Association (SIA) [http://public.itrs.net].
2) B. Yu, D. H. Ju, N. Kepler, T. J. King, and C. Hu: Proc. IEEE Symp. VLSI Technology, 1997, p. 105.
3) K. Chen, M. Chan, P. K. Ko, C. Hu, and J. H. Huang: Solid-State Electron. **38** (1995) 1975.
4) N. D. Arora, R. Rios, and C. L. Huang: IEEE Trans. Electron Devices **42** (1995) 935.
5) J. R. Pfiester, F. K. Baker, T. C. Mele, H. H. Tseng, P. J. Tobin, J. D. Hayden, J. W. Miller, C. D. Gunderson, and L. C. Parrillo: IEEE Trans. Electron Devices **37** (1990) 1842.
6) S. Iwata, N. Yamamoto, N. Kobayashi, T. Terada, and T. Mizutani: IEEE Trans. Electron Devices **31** (1984) 1174.

7) S.-I. Ohfuji, C. Hashimoto, T. Amazawa, and J. Murota: J. Electrochem. Soc. **131** (1984) 446.
8) Q. Lu, Y.-C. Yeo, P. Ranade, H. Takeuchi, T.-J. King, and C. Hu: Proc. IEEE Symp. VLSI Technology 2000, p. 72.
9) B. Cheng, B. Matti, S. Samayedam, J. Grant, B. Taylor, P. Tobin, and J. Mogab: Proc. IEEE Int. SOI Conf., 2001, p. 91.
10) B.-Y. Tsui and C.-F. Huang: IEEE Electron Device Lett. **24** (2003) 153.
11) C.-F. Huang and B.-Y. Tsui: Proc. Int. Conf. Microelectronics (MIEL), 2004, Vol. 2, p. 451.
12) B. C. Giessen, R. H. Kane, and N. J. Grant: Trans. Met. Soc. AIME **233** (1965) 855.
13) H. Zhong, S.-N. Hong, Y.-S. Suh, H. Lazar, G. Heuss, and V. Misra: IEDM Tech. Dig., 2001, p. 467.
14) V. Misra, H. Zhong, and H. Lazar: IEEE Electron Device Lett. **23** (2002) 354.
15) J. Lee, H. Zhong, Y.-S. Suh, G. Heuss, J. Gurganus, B. Chen, and V. Misra: IEDM Tech. Dig., 2002, p. 359.
16) K. G. Anil, A. Veloso, S. Kubicek, T. Schram, E. Augendre, J.-F. de Marneffe, K. Devriendt, A. Lauwers, S. Brus, K. Henson, and S. Biesemans: Proc. Symp. VLSI Techonolgy Dig., 2004, p. 190.
17) P. Xuan and J. Bokor: IEEE Electron Device Lett. **24** (2003) 634.
18) J. H. Sim, H. C. Wen, J. P. Lu, and D. L. Kwong: IEEE Electron Device Lett. **24** (2003) 631.
19) D. K. Schroder: *Semiconductor Material and Device Characterization* (Wiley, New York, 1998) 2nd ed., p. 347.
20) R. M. Waterstrat: Less-Common Met. **80** (1981) 31.
21) T. B. Massalski: *Binary Alloy Phase Diagrams* (American Society for Metals, Metals Park, OH, 1990) 2nd ed., p. 3133.
22) J. Chastain: *Handbook of X-ray Photoelectron Spectroscopy* (Perkin-Elmer, Waltham, MA, 1992), p. 170.
23) M. L. Steigerwald, R. M. Fleming, R. L. Opila, D. V. Lanf, R. B. Van Dover, and C. D. W. Jones: J. Appl. Phys. **91** (2002) 308.
24) N. J. Shevchik and D. Bloch: J. Phys. F **7** (1977) 543.
25) A. Jiang, A. Yohannan, N. O. Nnolim, T. A. Tyson, L. Axe, S. L. Lee, and P. Cote: Thin Solid Films **437** (2003) 116.
26) X. Chen, H. L. Frisch, and A. E. Kaloyeros: J. Vac. Sci. Technol. B **16** (1998) 2887.
27) H. P. Klug and L. E. Alexander: *X-ray Diffraction Procedure for Polycrystalline and Amorphous Materials* (Wiely, New York, 1974) 2nd ed., p. 656.
28) D.-Z. Xie, D.-Z. Zhu, and P.-X. Cao: J. Phys.: Condens. Matter **9** (1997) 4377.
29) F. K. Baker, J. R. Pfiester, T. C. Mele, H.-H. Tseng, P. J. Tobin, J. D. Haydenm, C. D. Gunderson, and L. C. Parrillo: IEDM Tech. Dig., 1989, p. 443.